Journal of Structural Biology 205 (2019) 26–33

Contents lists available at ScienceDirect

Journal of Structural Biology

journal homepage: www.elsevier.com/locate/yjsbi

Crystal structures of aminotransferases Aro8 and Aro9 from *Candida albicans* and structural insights into their properties

Agnieszka Kiliszek[a], Wojciech Rypniewski[a], Kamila Rząd[b], Sławomir Milewski[b], Iwona Gabriel[b,*]

[a] Institute of Bioorganic Chemistry, Polish Academy of Sciences, Noskowskiego 12-14, 61-704 Poznań, Poland
[b] Department of Pharmaceutical Technology and Biochemistry, Gdańsk University of Technology, Narutowicza 11/12, 80-233 Gdańsk, Poland

ARTICLE INFO

Keywords:
Aminotransferase
Multi-substrate enzyme
Pyridoxal-5′-phosphate
Crystal structure
X-ray crystallography

ABSTRACT

Aminotransferases catalyze reversibly the transamination reaction by a ping-pong bi-bi mechanism with pyridoxal 5′-phosphate (PLP) as a cofactor. Various aminotransferases acting on a range of substrates have been reported. Aromatic transaminases are able to catalyze the transamination reaction with both aromatic and acidic substrates. Two aminotransferases from *C. albicans*, Aro8p and Aro9p, have been identified recently, exhibiting different catalytic properties. To elucidate the multiple substrate recognition of the two enzymes we determined the crystal structures of an unliganded *Ca*Aro8p, a complex of *Ca*Aro8p with the PLP cofactor bound to a substrate, forming an external aldimine, *Ca*Aro9p with PLP in the form of internal aldimine, and *Ca*Aro9p with a mixture of ligands that have been interpreted as results of the enzymatic reaction. The crystal structures of both enzymes contains in the asymmetric unit a biologically relevant dimer of 55 kDa for *Ca*Aro8 and 59 kDa for *Ca*Aro9p protein subunits. The ability of the enzymes to process multiple substrates could be related to a feature of their architecture in which the active site resides on one subunit while the substrate-binding site is formed by a long loop extending from the other subunit of the dimeric molecule. The separation of the two functions to different chemical entities could facilitate the evolution of the substrate-binding part and allow it to be flexible without destabilizing the conservative catalytic mechanism.

1. Introduction

Aminotransferases catalyze reactions in the amino acid biosynthesis and other metabolic pathways in almost all prokaryotes and eukaryotes. The enzymes catalyze the interconversion of amino acids and oxoacids by a transfer of amino group. Aminotransferases utilize pyridoxal-5′-phosphate (PLP) as a coenzyme in the transit of the amino groups. In the resting enzyme the aldehyde group of PLP forms an imine linkage (internal aldimine) with the ε-amino group of a specific lysine residue in the protein. In the presence of an amino acid substrate the link is disrupted and an imine (external aldimine) is formed between the coenzyme and the substrate. This is then hydrolyzed to release a 2-oxocarboxylate product leaving the coenzyme in the form of a pyridoxamine. The process can be reversed with another oxoacid to restore the enzyme to its initial form (Fig. 1).

Aminotransferases can be exclusive for a particular pathway or they can have multiple catalytic capabilities with functional overlaps between different cellular processes. Aro8 and Aro9 were initially identified as aromatic aminotransferases I and II from *S. cerevisiae* (*Sc*Aro8p and *Sc*Aro9p) (Iraqui et al., 1998; Urrestarazu et al., 1998). In biochemical studies, *Sc*Aro8p was found to exhibit a broad substrate specificity, similar to many class I aminotransferases, and has been reported to utilize glutamate, phenylalanine, tyrosine and tryptophan as amino donors, with phenylpyruvate (PhePi), 4-hydroxyphenylpyruvate, 2-oxoglutarate and pyruvate as amino acceptors (Iraqui et al., 1998; Karsten et al., 2011; Kradolfer et al., 1982; Urrestarazu et al., 1998). In addition, it can use methionine, leucine, and α-aminoadipate as amino donors, with their corresponding 2-oxo acids as acceptors. The authors postulated that *Sc*Aro8p played an essential role in the synthesis of phenylalanine and tyrosine. In comparison, they considered Aro9 to be mainly involved in tryptophan degradation and as an inducible catabolic enzyme that nevertheless catalyzes the formation of Phe and Tyr in *S. cerevisiae* Δaro8 mutants. Further evidence supported a reclassification of *Sc*Aro8p as an α-aminoadipate aminotransferase in the biochemical pathway of lysine synthesis. This is based on a recent study in which the enzyme was

Abbreviations: AA, 2-aminoadipate; BTB, bis-tris methane; LLP, lysine-pyridoxal-5′-phosphate; PLP, pyridoxal-5′-phosphate; PMP, pyridoxamine-5′-phosphate; PhePi, 3-phenylpyruvic acid; PEG, polyethylene glycol; MPD, 2-methyl-2,4-pentanediol

* Corresponding author.
E-mail address: iwogabri@pg.edu.pl (I. Gabriel).

https://doi.org/10.1016/j.jsb.2019.02.001
Received 5 October 2018; Received in revised form 4 January 2019; Accepted 3 February 2019
Available online 08 February 2019

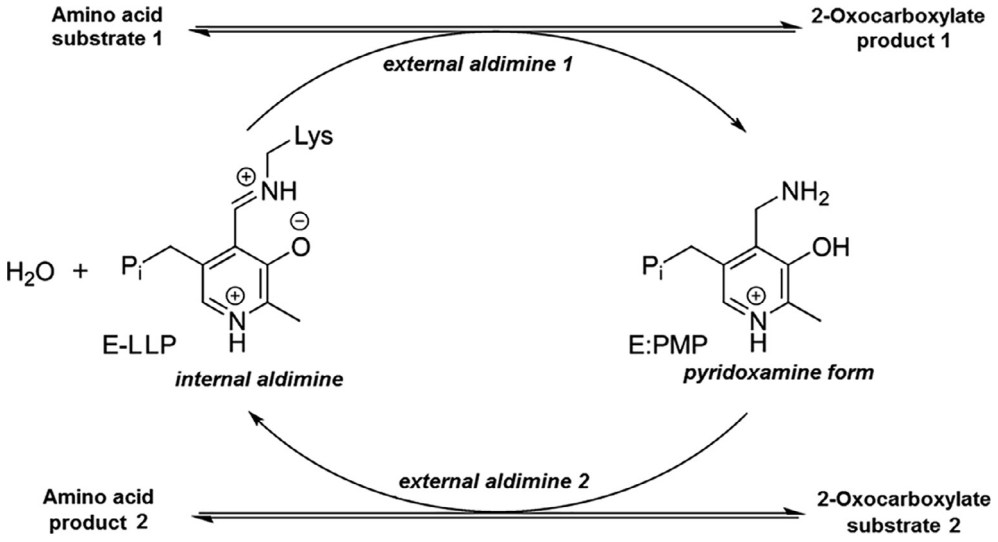

Fig. 1. The general reaction scheme of aminotransferases (transaminases) containing pyridoxal phosphate as a cofactor.

Table 1
Summary of X-ray data collection and crystallographic models.

	*Ca*Aro8p	*Ca*Aro8p + ligands	*Ca*Aro9p	*Ca*Aro9p + ligands
PDB code	6HNB	6HNU	6HND	6HNV
Space group	$P2_12_12_1$	$P2_12_12_1$	$P2_12_12_1$	$P2_12_12_1$
Cell parameters *a, b, c* [Å]	70.4, 102.3, 147.1	69.8, 102.1, 146.9	75.4, 89.3, 161.9	74.6, 88.5, 161.0
Resolution [Å]	1.96	1.80	2.23	2.60
No. unique refl.	76,417	97,014	53,903	31,583
Completeness [%]	99.4 (96.6)	99.6 (98.6)	99.7 (99.1)	94.0 (95.7)
Redundancy	7.1 (7.0)	4.1 (4.1)	6.0 (5.9)	4.7 (4.7)
I/σ(I)	13.0 (2.0)	11.3 (1.9)	11.3 (2.2)	9.2 (2.0)
R_{merge} [%]	14.8 (1 0 0)	9.7 (71.3)	15.4 (91.9)	17.8 (90.4)
R/R_{free} [%]	17.2/23.3	17.4/21.9	16.9/23.0	19.9/28.0
r.m.s. bonds [Å]	0.018	0.010	0.008	0.007
r.m.s. angles [°]	1.8	1.6	1.5	1.6
Protein content	Chain A: 480 res. Chain B: 479 res.	Chain A: 479 res. Chain B: 480 res.	Chain A: 467 res. Chain B: 470 res.	Chain A: 467 res. Chain B: 467 res.
Ligands	2 × sulfate 2 × bis-tris-methane 1 × Cl^-	2 × pyridoxal phosphate 2 × phenylalanine 1 × tris 2 × bis-tris methane	2 × bound pyridoxal phosphate 2 × MPD 1 × K^+	2 × bound pyridoxal phosphate 1 × phenylalanine 1 × 3-phenylpyruvate 1 × α-aminoadipate 1 × 2-oxoadipate 3 × bicine 1 × MPD
Ordered solvent water molecules	948	1128	520	195

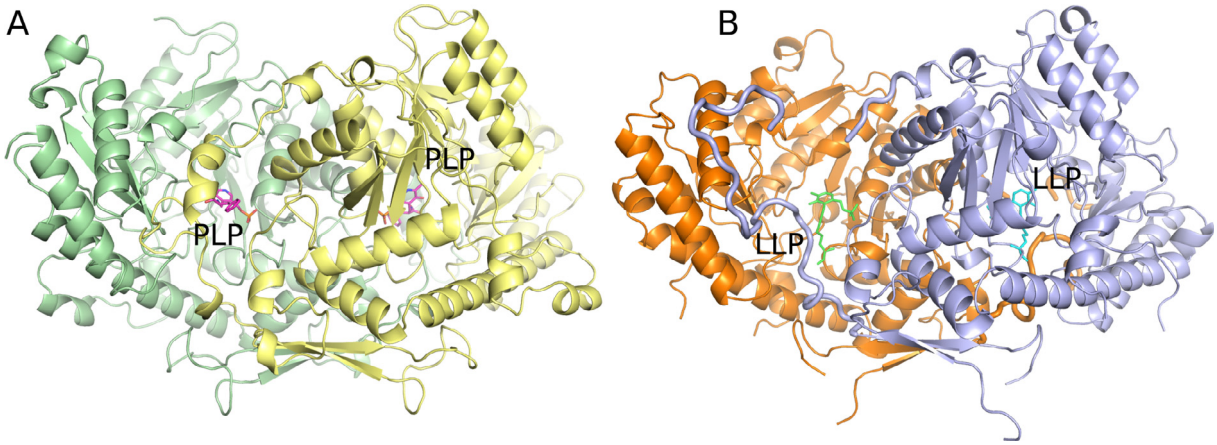

Fig. 2. Cartoon representation of *Ca*Aro8p dimer (A), *Ca*Aro9p dimer (B). Cofactors and bound ligands are shown as sticks.

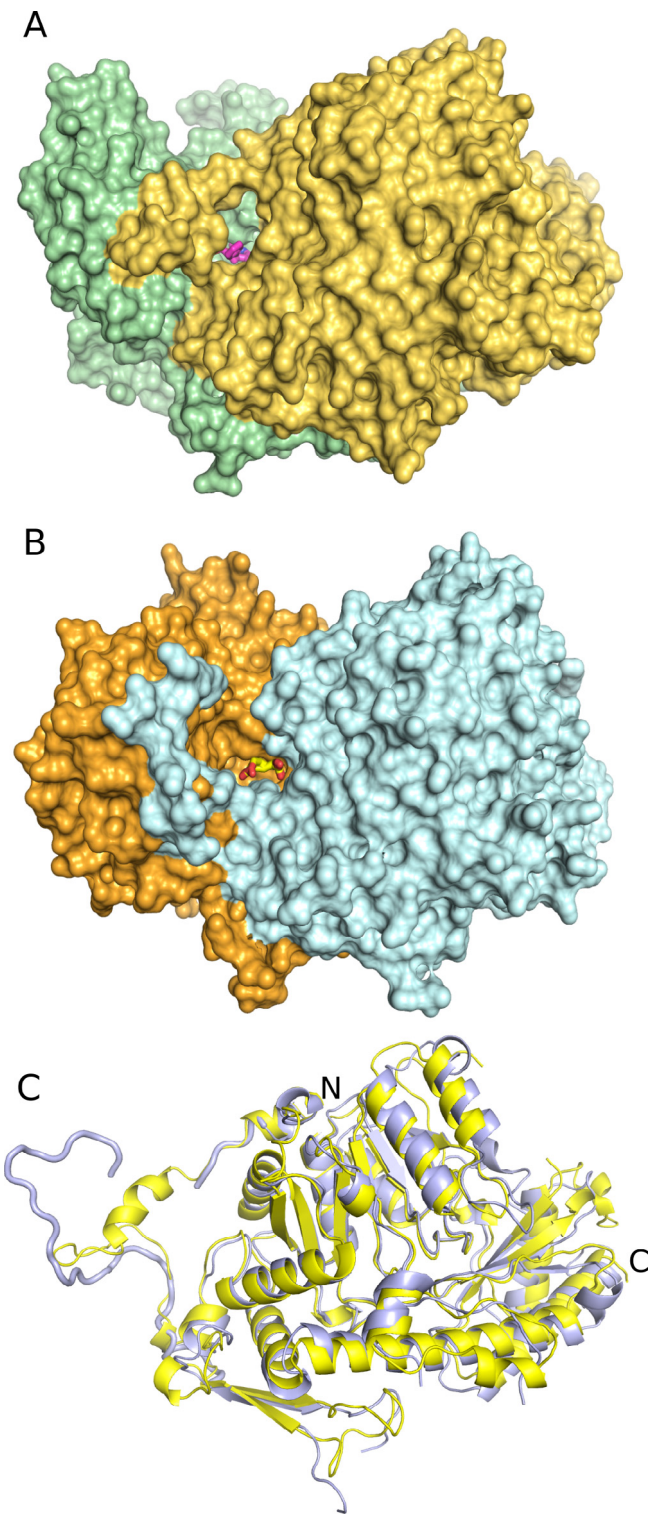

Fig. 3. Surface representation of a *Ca*Aro8p dimer (A) and a *Ca*Aro9p dimer (B), showing one of the active site cavities. Subunits of the dimeric molecules are shown in different colors. Bound ligands are shown as sticks: Phe in the case of *Ca*Aro8p and α-aminoadipate and the corresponding oxocarboxylic acid bound to *Ca*Aro9p. The PLP/LLP cofactors (not shown) are bound to one subunit while the ligand-binding sites are formed by the other subunit. The largest differences between the two enzymes are in the N-terminal segments that extend over to the other subunit. This is most evident on the ribbon diagram of superposition of *Ca*Aro8p (*yellow*) and *Ca*Aro9p (*blue*) subunits (C). The ligand-binding site is larger in *Ca*Aro9p then in *Ca*Aro8p.

shown to display a greater specificity towards 2-oxoadipate compared to the aromatic amino acid substrates, such as phenylalanine and tyrosine (Karsten et al., 2011). In contrast to *S. cerevisiae*, *C. glabrata* uses histidine as the sole source of nitrogen and the aromatic amino acid aminotransferase Aro8, but not Aro9, is required for this process *in vivo* (Brunke et al., 2014).

The recently identified Aro8p from *Candida albicans* (*Ca*Aro8p) has been found to participate in lysine, aromatic amino acids and histidine degradation as well as in the biosynthesis of Lys, Phe and Tyr. *Ca*Aro9p appears to be an auxiliary enzyme, participating in the catabolism of aromatic amino acids and lysine at high concentrations of these compounds, with no biosynthetic role (Rzad and Gabriel, 2015; Rzad et al., 2018).

Only limited structural data are available for the fungal aromatic aminotransferases. The crystal structure of *Sc*Aro8p, obtained in the absence of ligands, has been recently determined at 1.91 Å resolution (PDB ID: 4JE5) (Bulfer et al., 2013). The active site revealed an asymmetric cofactor binding with the pyridoxal-5-phosphate (PLP) covalently linked to a lysine residue in one subunit of the *Sc*Aro8p homodimer, while the other subunit contained pyridoxamine phosphate (PMP) and a HEPES buffer molecule. The structure of *Sc*Aro8 adopted a typical type-1 aminotransferase fold, comprising large (residues 52–368) and small (residues 369–500) domains, both of mixed α/β topology.

To gain insight into the structural basis of the activities of *Ca*Aro8p and *Ca*Aro9p we have determined and compared the crystal structures of both enzymes with cofactors and selected ligands. The structure of *Ca*Aro8p is the first aromatic aminotransferase from a pathogenic fungus, thus it is a possible drug target, while the structure of *Ca*Aro9 is the first determined structure of Aro9 aminotransferase.

2. Materials and methods

2.1. Strains and growth conditions

E. coli TOP 10F' strain from Invitrogen was used in cloning procedures. *E. coli* Rosetta (DE3) pLysS strain from Novagen was used for the overproduction of wild type *Ca*Aro8p and *E. coli* BL21 Star (DE3) cells were used for the heterologous expression C-oligoHis-tagged *Ca*Aro9CHp. *E. coli* strains were cultured at 37 °C on LB (Luria–Bertani) solid medium [1.0% (w/v) NaCl, 1.0% (w/v) tryptone, 0.5% yeast extract and 1.5% (w/v) agar] and LB liquid medium supplemented with 100 μg ml^{-1} ampicillin and/or 34 μg ml^{-1} chloramphenicol, when required.

2.2. Subcloning, protein expression and purification

Cloning of *ARO9CH* was performed as previously described for *ARO8* (Rzad and Gabriel, 2015) and *ARO9* (Rzad et al., 2018) with the use of the pET Directional TOPO Expression Kit and the pET101/D-TOPO plasmid (Invitrogen). The fragment of the *ARO9* gene was amplified from the *C. albicans* SC5314 genomic DNA by PCR. The primers used in the amplification were: ARO9.f 5′-CACCATGTCTGATCCTACT CATTTAATTTCTAAG-3′ and ARO9CH.r 5′- CTTTTTA**ATGATGATGAT GATGATG**AAACTCTAACCC-3′. The hexaHis-tag-encoding sequence introduced in the reversed primer is bolded. Primers were designed according to the manufacturer's instruction. The PCR products were purified from an agarose gel and cloned directionally into the pET101/D-TOPO vector, thus yielding the recombinant expression plasmid pET101/D-TOPO + *ARO9CH*. Conditions for *E. coli* transformation, overexpression of *CaARO8* and isolation of *Ca*Aro8p were the same as described previously (Rzad and Gabriel, 2015). The overexpression of Ca*ARO9CH* was performed as described previously for wild type enzyme *Ca*Aro9p (Rzad et al., 2018) although the purification of the oligoHis-tagged *Ca*Aro9p was performed by metal-affinity chromatography. Bacterial pellet was resuspended in buffer A (20 mM Tris-HCl,

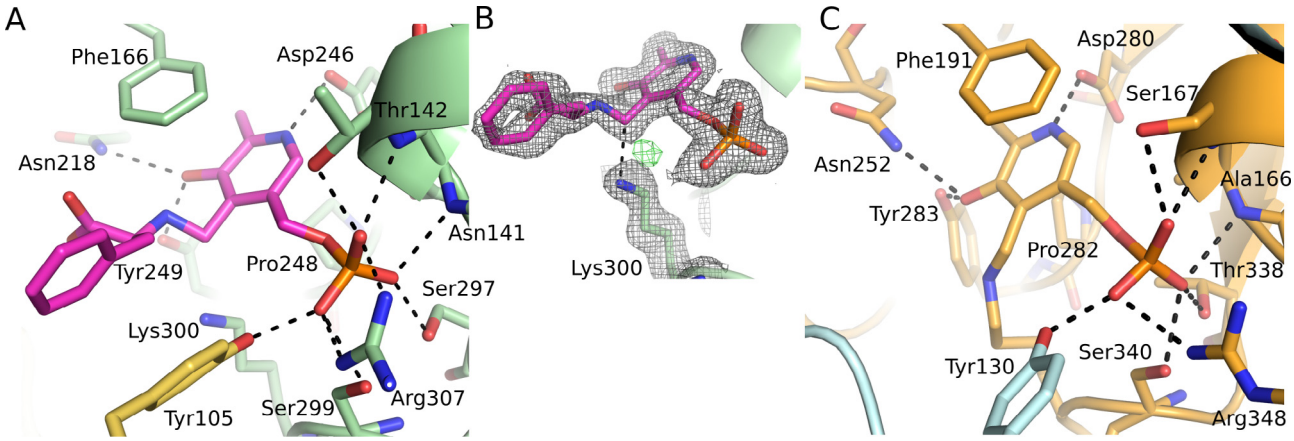

Fig. 4. Protein interactions with the cofactor. PLP forms an external aldimine with Phe (*pink sticks*) in *Ca*Aro8p. Hydrogen bonds between the protein and the cofactor are shown as dotted lines (A). $2F_o$-F_c electron density (*grey*, contoured at 1σ level) of the external aldimine and the catalytic Lys300 in *Ca*Aro8p. A residual peak in the F_o-F_c difference density (*green*, contoured at 3σ) indicates that a minor fraction of the molecules in the crystal has the form of an internal aldimine, making a covalent bond with Lys300 (B). PLP forming an internal aldimine with *Ca*Aro9p (C).

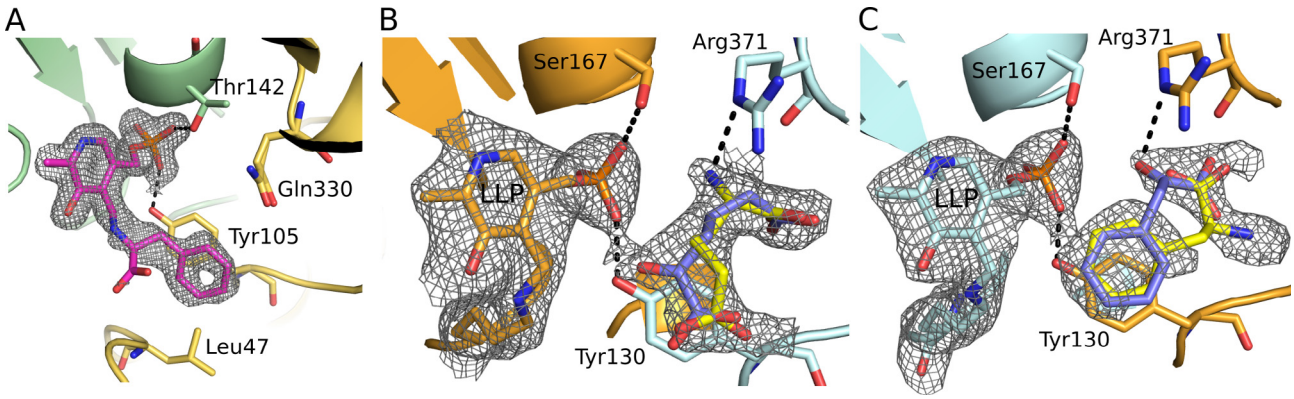

Fig. 5. Protein interactions with ligands. Electron density (*mesh*) corresponds to a Phe residue bound covalently (forming an external aldimine) to the PLP cofactor in the ligand-binding cavity of *Ca*Aro8p. The cofactor is bound to subunit B (in the depth of the picture, not shown), while the Phe ligand is surrounded by residues of subunit A. The contours show the electron density at the 1σ level (A). α-Aminoadipate and the corresponding oxocarboxylic acid bound to *Ca*Aro9p (B), PhePi/Phe bound to *Ca*Aro9p (C).

pH 8, 5 mM imidazole, 0.6 M NaCl and 0.5 mM phenylmethylsulfonyl fluoride/PMSF/) and the cells were disrupted by sonication (Branson sonifier 250) on ice. The total lysate was centrifuged at 16,000 × g for 20 min, at 4 °C. The supernatant (crude extract) was applied to a HisTrapFF column which was pre-equilibrated with buffer A. The oligoHis-tagged proteins were eluted by increasing concentrations of imidazole in elution buffer B (20 mM Tris-HCl, pH 8, 500 mM imidazole, 0.5 M NaCl, gradient of buffer A and B: 0–100%). For further assays, the eluates were concentrated by ultrafiltration using Vivaspin concentrators (10 kDa cut-off limit; Viva Science Ltd.) at 7000 × g for 30 min. *Ca*Aro8p and *Ca*Aro9CHp were further purified by gel filtration chromatography using a Superdex 200 column (GE Healthcare) equilibrated in 20 mM Tris-HCl buffer, pH 8.0 with 150 mM NaCl. After purification, the proteins were judged to be essentially pure by SDS-PAGE. Oligomeric structure of *Ca*Aro9p was analysed by the size-exclusion chromatography performed on Superdex 200 HR 10/30 and native PAGE electrophoresis using the NativePAGE Novex 4–16% Bis-Tris Gels kit (Invitrogen). The experiments were run according to the manufacturer's procedure.

2.3. Crystallization and structure determination

Colorless crystals of native *Ca*Aro8p were obtained by sitting drop vapor diffusion at 19 °C by mixing 2:1 ratio of 9 mg/mL protein with 0.2 M $MgCl_2$, 0.1 M Bis-Tris pH 5.5, 25% PEG 3350. The crystals of the enzyme-ligands complex were obtained by soaking the crystals (obtained by mixing 2:1 ratio of 12 mg/mL protein with the same crystallization buffer) in 6 mM PLP and 5.5 mM PhePi. Yellow crystals of *Ca*Aro9p containing LLP were obtained by sitting drop vapor diffusion at 19 °C by mixing 1:1 ratio of 18 mg/mL protein with 0.06 M $MgCl_2$, 0.06 M $CaCl_2$, 0.1 M Tris (base): BICINE pH 8.5, 12.5% v/v MPD, 12.5% PEG 1000, 12.5% w/v PEG 3350. Crystals of the *Ca*Aro9p complex with ligands were obtained by co-crystallization of the protein with a two-fold molar excess of PhePi and AA. The crystals were picked with a cryoloop directly from the crystallization drop and placed immediately in a stream of cold nitrogen gas. No additional cryoprotectant was used.

X-ray diffraction data were collected on BL14.2 and BL14.3 at the BESSY II electron storage ring (Mueller et al., 2015) on the Pilatus2M and MX-225 detectors, respectively. The crystals throughout the data collected were kept at the temperature of 100 K by a stream of cold nitrogen gas. The data were processed using XDS (Kabsch, 2010). The structure of *Ca*Aro8p was solved by molecular replacement using the program Phaser (Mccoy et al., 2007) and with the structure of *Sc*Aro8p (PDB ID: 4JE5) (Bulfer et al., 2013) as the search model. The structure of *Ca*Aro9p was solved similarly by molecular replacement, but the *Sc*Aro8p search model had the amino acid side chains truncated to Ala. The initial models having the correct amino acid sequence were build using the Arp/wArp server (Langer et al., 2008), refined using Refmac5 (Murshudov et al., 1997), belonging to the CCP4 program suite (Winn et al., 2011), and inspected and corrected using Coot (Emsley et al.,

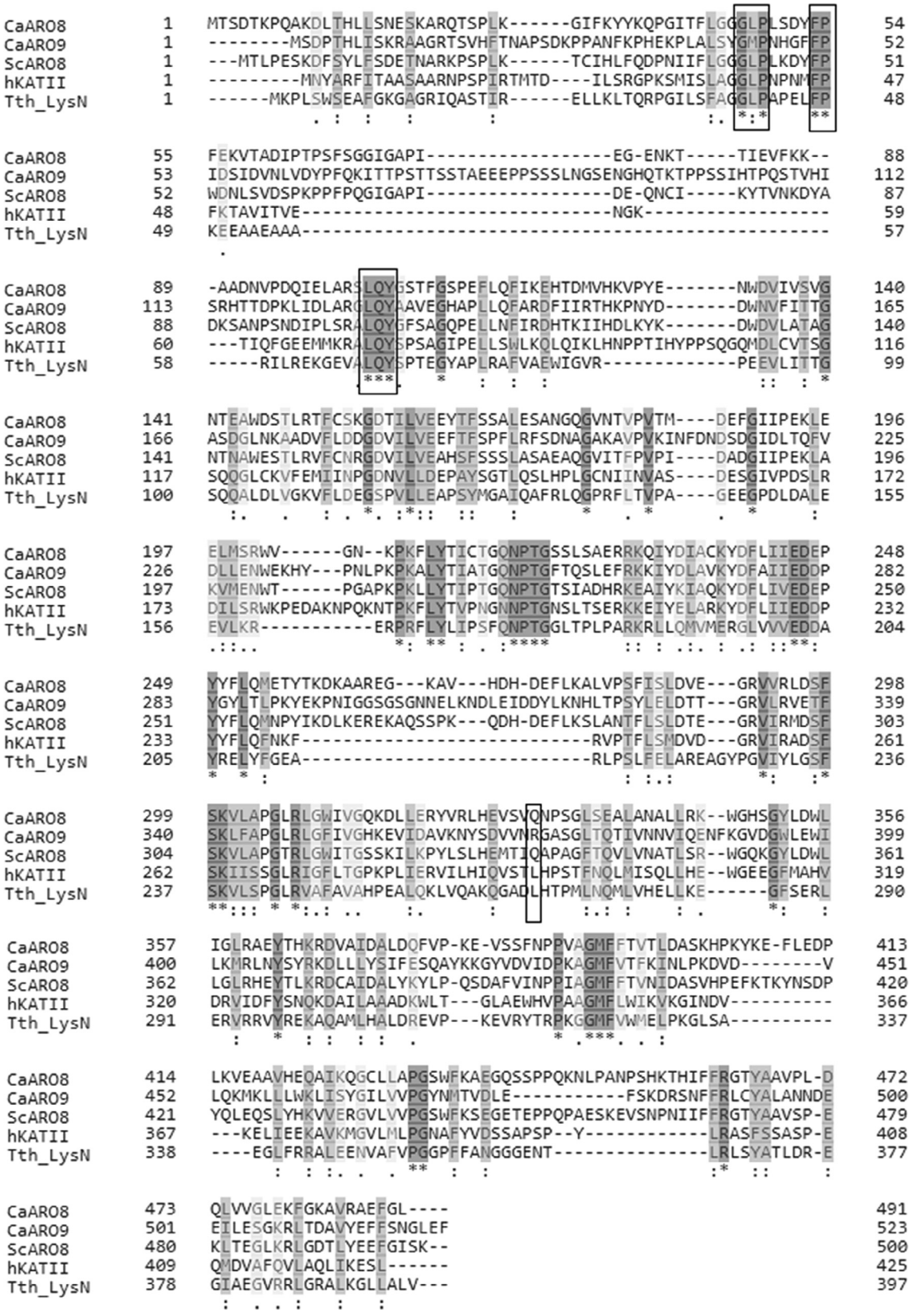

Fig. 6. Multiple alignment of amino acid sequences of transaminases exhibiting α-aminoadipate or aromatic aminotransferase activity from *C. albicans* (*Ca*ARO8 and *Ca*ARO9), *S. cerevisiae* (ScARO8), *T. thermophilus* (Tth_LysN) and human (hKATII). Highly conserved residues are marked as (*). Three conserved sequence motifs in the N-terminal loop whose mutual interactions stabilize one side of the ligand-binding site and the active Lys residue in *Ca*Aro8p and *Ca*Aro9p as well as non-conserved site that has been proposed to play a role in substrate recognition are framed in black.

2010). The X-ray data and molecular models are summarized in Table 1.

PDB ID: 6HNB, 6HND, 6HNU, 6HNV

3. Results and discussion

The presented results include the first structure of an aromatic aminotransferase Aro8p in the form of external aldimine and the first crystal structure of Aro9p. Only one other protein structure from a eukaryotic source, exhibiting aromatic aminotransferase activity is known: Aro8p from *S. cerevisiae* (PDB ID: 4JE5) (Bulfer et al., 2013). *Ca*Aro8p and *Ca*Aro9p structures are the first structures of aromatic aminotransaminases from the pathogenic fungus *Candida albicans*.

3.1. Overall structure of CaAro8p and CaAro9p

The crystal structure of *Ca*Aro8p contains in the asymmetric unit a biologically relevant dimer of 55 kDa protein subunits, each 491 amino acid residues long (Fig. 2A) (Rzad and Gabriel, 2015). The electron density of the main chain is continuous except the first five N-terminal residues and residues 450–456, which are disordered. The fold is similar to Aro8 from *Saccharomyces cerevisiae* (Bulfer et al., 2013) with which it shares 53% sequence identity and is characteristic of class 1 pyridoxal-phosphate-dependent aminotransferase family (Paiardini et al., 2004). Each subunit consists of two domains, each with a β-sheet at its core, surrounded by α-helices, 3_{10}-helices and loops (Fig. S1A). The N-terminal domain is preceded by a 50-residue loop that extends over the surface of the other subunit, covering part of its substrate-binding site. Then follow two anti-parallel β-strands that interact with the corresponding strands of the other subunit to form a 4-straded β-sheet. The main fold of the N-terminal domain (residues 109–347) consists of a 7-stranded β-sheet in which the strands have mixed parallel and anti-parallel orientations. They are connected by α-helices, 3_{10} motifs and turns. The N- and C-terminal domains are connected by a helix (α13, residues 348–377). The C-terminal domain (residues 363–491) consists of a 4-stranded anti-parallel β-sheet adhering on one side to the larger domains and on the outer side covered by three α-helices: α13, α14 and α15. The segment 450–456, between the last two β-strands, is disordered, showing no interpretable electron density.

Structural comparison with the only known structure of aromatic aminotransferase from *S. cerevisiae* (*Sc*Aro8p) (PDB ID: 4JE5) indicates close structural similarity between the two proteins. The largest differences occur in loops located on the protein's surface. There is also a shift by approximately 2.5 Å of residues 29–40 in *Ca*Aro8p, compared to residues 26–37 of one subunit in each of the two *Sc*Aro8p crystallographic dimers (Fig. S2). This segment of the amino acid sequence is at the entrance to the substrate-binding site and the shift makes the cavity narrower in *Sc*Aro8p. It is difficult to assess the significance of this change because in *Sc*Aro8p this region is involved in crystal contacts with neighboring protein molecules, and in the other subunit of each *Sc*Aro8p dimer the segment is partly disordered, having unknown atomic coordinates. Most residues of the segment are not conserved. It is possible that substrate specificity of the related Aro8 enzymes is modulated by this part of the protein structure.

The crystal structure of *Ca*Aro9p contains in the asymmetric unit a dimer of 59 kDa protein subunits, each 523 amino acids residues long (Fig. 2B). The results are consistent with the oligomeric structure of the enzyme obtained on the basis of experimental data (data not shown). The overall topology is similar to *Ca*Aro8p, with some differences (Fig. S1B). The electron density is well-defined except for the three segments: residues 19–24 in the loop that extends over the neighboring subunit, residues 69–104 in an extended loop absent in *Ca*Aro8p, between strands β2 and β3, and residues 296–309 following the β10 strand. *Ca*Aro9p has a longer N-terminal loop than *Ca*Aro8p, and part of the loop, as mentioned above, is disordered. As a result, the active site in *Ca*Aro9p is less occluded than in *Ca*Aro8p (Fig. 3).

3.2. Cofactor binding

When comparing the crystal structures of *Ca*Aro8p and *Ca*Aro9p, the first observation is that when *Ca*Aro8p was purified in the absence of the cofactor, it crystallized in the apo form, and when the crystals of *Ca*Aro8p were soaked with the cofactor and ligands, the enzyme formed a stable external aldimine. On the other hand, *Ca*Aro9p copurified with the cofactor and in the crystal structure it has the form of an internal aldimine regardless of the presence or absence of ligands in the crystallization buffer. A possible explanation of the difference in the enzymes' interactions with PLP is that ammonium sulfate precipitation was used in the purification of *Ca*Aro8p but not *Ca*Aro9p, thus it is possible that the cofactor was lost at that stage from the unliganded *Ca*Aro8p structure and replaced by a sulfate anion observed in the *Ca*Aro8p structure obtained in the absence of ligands.

In the *Ca*Aro8p + ligands structure, the cofactor has predominantly the form of an imine (external aldimine) between pyridoxal phosphate and a ligand. The cofactor is lodged in each of the larger domains, at the ends of β-strands β10 and β11, and the start of helix α5, which points at the phosphate moiety, stabilizing its negative charge with the positive end of the helix dipole. There are direct contacts between two of the phosphate's oxygen atoms and the main chain's NH groups of residues 141 and 142 at the start of the helix (Fig. 4A). It is further stabilized by the side chains of Thr142, Ser297 and Ser299. Another stabilizing interaction is the salt bridge between the phosphate and the guanidinium group of Arg307. The pyridoxal ring is wedged between Phe166 and Pro248. In addition, there is a salt bridge between the pyridine N atom and the carboxylate group of Asp246 and an H-bond between the O3 atom and the hydroxyl group of Tyr249. All the interactions with the cofactor are conserved in comparison with Aro8 from *S. cerevisiae* (Bulfer et al., 2013). Lys300, known to participate in the enzymatic reaction by forming an internal aldimine with the pyridoxal phosphate, has been modelled as separate from the cofactor (Fig. 4B). The N-C distance between the lysine's amino group and the cofactor's C4 atom is 2.6–2.7 Å. There is however a residual positive electron density, at the level of 3.5–4.0 σ in the F_{obs}-F_{calc} difference map, indicating that a minor proportion of the molecules in the crystal forms an imine bond with Lys300.

In the *Ca*Aro9p structure, obtained with no added ligands, there is a pyridoxal phosphate bound to the catalytic Lys341, forming an inner aldimine. The covalent bond between the carbonyl group of the pyridoxal and the amine group of the lysine is evidenced by a clear electron density. The residues coordinating the cofactor are conserved in comparison with *Ca*Aro8p, except for Ser167 in *Ca*Aro9p which replaces Thr142 in *Ca*Aro8p, but the H-bonds formed by the residues' hydroxyl groups are maintained (Fig. 4C).

3.3. Substrate binding site

In *Ca*Aro8p + ligands, obtained in the presence of PLP and PhePi, there is a continuous electron density in both protein subunits, extending from the pyridoxal rings into the substrate-binding pockets, indicating that an imine has formed with an external ligand, which has been modelled as a phenylalanine because a phenyl ring can be discerned (Fig. 5A). However, this interpretation is not fully satisfactory because of an additional unclear electron density at the side chain, indicating that the observed density is a superposition of at least two chemical species. Also, the carboxyl groups of the bound amino acid residues are poorly defined, which could be a result of their mobility. The ligand-binding cavity is formed entirely by residues of the N-terminal segment from the other subunit of the homodimer. The phenyl ring of the bound ligand stacks against the ring of Tyr105 (from the other subunit). It also makes a hydrophobic contact (3.2–3.4 Å) with Leu47 (also from the other subunit).

In the *Ca*Aro9p + ligands structure there is a clear electron density corresponding to the pyridoxal phosphate bound to Lys341, as

evidenced by a continuous electron density. In addition, there is a sizable electron density in the substrate-binding space. The ligand densities differ between the two subunits of the homodimer and in subunit A, the density was interpreted as a superposition of 2-aminoadipate (AA) and 2-oxoadipic acid (Fig. 5B), while in subunit B, the density was interpreted as a superposition of 3-phenylpyruvic acid (PhePi) and phenylalanine (Fig. 5C). The mixture of ligands can be interpreted as a results of the enzymatic reaction finding a balance between amination of PhePi and deamination of α-aminoadipate. This interpretation takes into account the content of the crystallization medium. AA and PhePi were present in the crystallization solution, while 2-oxoadipic acid and phenylalanine could be produced by the transamination reaction catalyzed by the enzyme. The interpretation of the ligand density in subunits B is based on an observation of a planar electron density stacked against Tyr 130, in which the phenyl ring could be fitted, while the corresponding place at chain A contained an elongated electron density, in which the aminoadipate and the oxo acid could be fitted. The ligands fit inside the density and make reasonable contacts with the protein, but one needs to bear in mind that interpretation of ligand density cannot be certain at 2.6 Å resolution.

Asymmetry between equivalent binding sites in an oligomer is unusual but has been observed before. The closest example is the crystal structure of Aro8 from *S. cerevisiae* (Bulfer et al., 2013). Asymmetry between the bound ligands is also visible *Ca*Aro8p + ligands as additional peaks in the electron density, but not clear enough for interpretation. The asymmetry could be related to the topology of Aro8/Aro9 is which the N-terminal segment of each subunit reaches across to the neighboring subunits to form its substrate-binding site. The N-terminal segments are also connected to form a common β-sheet. It is possible that this arrangement is finely balanced and the balance tips easily destroying the symmetry between the binding sites.

It is interesting that different complexes are formed upon addition of ligands to the two enzymes. The ligands had been selected in the hope of forming stable rather than reactive complexes but enzymatic reactions apparently have taken place in both crystal forms. The crystal structure shows that *Ca*Aro8p + ligands has stabilized in the state of external aldimine, while the structure of *Ca*Aro9p + ligands stabilized at the stage of internal aldimine, i.e. further along the path towards amino acid synthesis. One possibility is that this is the natural property of the protein to show a greater stability of this form, as opposed to *Ca*Aro8p which finds a balance at the external aldimine.

The most evident difference between *Ca*Aro8p and *Ca*Aro9p in their substrate binding areas is in the N-terminal parts of the amino acid chains which form the ligand-binding site and should have a role in gating access to the active site (Fig. 3). The loop is wider in *Ca*Aro9p than in *Ca*Aro8p due to an insertion of six residues (24–29) and disorder of residues 19–24 (Fig. 3C). It is probable that greater access to the active center results in weaker binding and, consequently, lower affinity for substrates. Consistently with this, the K_m parameters, determined *in vitro* for different substrates, are higher for *Ca*Aro9p than for *Ca*Aro8p (Rzad et al., 2018).

The sequence and structure comparisons between *Ca*Aro8p, *Ca*Aro9p and related enzymes indicate that the area around the ligand is rather variable and there are few specific interactions between the proteins and the ligands away from the immediate vicinity of the active site. The ligand-binding area is rimmed by the N-terminal loop of the neighboring subunit which, as already mentioned, is longer in *Ca*Aro9p than in *Ca*Aro8p and partly disordered. However, there are three conserved sequence motifs in the N-terminal loop whose mutual interactions stabilize one side of the ligand-binding site and the active Lys residue (Lys300 in *Ca*Aro8p and Lys341 in *Ca*Aro9p). These are residues 46–48, 53–54 and 103–105 in *Ca*Aro8p and correspondingly 44–46, 51–52 and 252–255 in *Ca*Aro9p (Fig. 6). Leu47 in *Ca*Aro8p is substituted by Met45 in *Ca*Aro9p, but this does not change the character of the residue. The other side of the ligand-binding area contains a non-conserved site that has been proposed to play a role in substrate recognition in related enzymes. The human aminoadipate aminotransferase/kynurenine aminotransferase II (hKATII) contains Leu293 in the corresponding position (PDB ID: 2ZP7) (Han et al., 2008) while α-aminoadipate aminotransferase from *Thermus thermophilus* (*Tth*LysN) has Leu268 there proposed to interact with the substrate molecule 2-oxoglutarate (PDB ID: 3DC1) (Tomita et al., 2009). *Ca*Aro8p and *Sc*Aro8p have a Gln residue in this position, Gln330 and Gln335, respectively, while in *Ca*Aro9 this site contains Arg371. In the crystal structures, both Gln330 in *Ca*Aro8p and Arg371 in *Ca*Aro9p are close to the ligands (Fig. 5). Kinetic parameters of catabolic and anabolic reactions catalyzed by *Ca*Aro8p and *Ca*Aro9p revealed significant differences between the two enzymes. The latter is not able to use histidine as amino group donor (with 2-oxoglutarate) and catalyze anabolic reactions with phenylpyruvate or 4-hydroxyphenylpyruvate with L-Glu as amino group donor (Rzad et al., 2018). Arg371 in *Ca*Aro9p, would change the electrostatic character of the ligand-binding area and is likely to play a role in substrate recognition, although future experiments are required to confirm that assumption

4. Conclusions

Enzymatic studies showed that *Ca*Aro8p and *Ca*Aro9p are not specific for particular substrates but instead show different levels of reactivity against a range of amino- or oxoacids. The crystal structures corroborate these results by revealing structures that contain well defined and conserved active sites, while the substrate-binding surroundings are rather variable or even showing a degree of disorder. The largest differences between *Ca*Aro8p and *Ca*Aro9p are in the N-terminal parts of the amino acid chains which extend over to the other subunit as well as form the ligand-binding site and should have a role in gating access to the active site. It is interesting that the catalytic function is located on one subunit while the substrate binding function resides on the other subunit. Separate chemical entities, even when they are in contact, are probably less interdependent in terms of structure and stability than adjacent elements within a single folded subunit. It is possible that this separation facilitates evolution of the substrate-binding part without affecting the catalytic mechanism. It could also allow a promiscuity of the enzyme towards substrates by means of an increased flexibility/disorder of the substrate binding part, without necessarily destabilizing the conserved parts of the structure that carry out the enzymatic reaction.

Acknowledgements

Diffraction data have been collected on BL14.2 and BL14.3 at the BESSY II electron storage ring operated by the Helmholtz-Zentrum Berlin (Mueller et al., 2015). We would particularly like to acknowledge the help and support of Manfred Weiss during the experiment. Financial support for these studies by the National Science Centre, Poland (grant No. 2015/17/B/NZ6/04248 awarded to IG) is gratefully acknowledged.

Appendix A. Supplementary data

Supplementary data to this article can be found online at https://doi.org/10.1016/j.jsb.2019.02.001.

References

Brunke, S., Seider, K., Richter, M.E., Bremer-Streck, S., Ramachandra, S., Kiehntopf, M., Brock, M., Hube, B., 2014. Histidine degradation via an aminotransferase increases the nutritional flexibility of Candida glabrata. Eukaryot. Cell 13, 758–765.

Bulfer, S.L., Brunzelle, J.S., Trievel, R.C., 2013. Crystal structure of Saccharomyces cerevisiae Aro8, a putative alpha-aminoadipate aminotransferase. Protein Sci.. 22, 1417–1424.

Emsley, P., Lohkamp, B., Scott, W.G., Cowtan, K., 2010. Features and development of Coot. Acta Crystallogr. D Biol. Crystallogr. 66, 486–501.

Han, Q., Cai, T., Tagle, D.A., Robinson, H., Li, J.Y., 2008. Substrate specificity and structure of human aminoadipate aminotransferase/kynurenine aminotransferase II.

Biosci. Rep. 28, 205–215.
Iraqui, I., Vissers, S., Cartiaux, M., Urrestarazu, A., 1998. Characterisation of Saccharomyces cerevisiae ARO8 and ARO9 genes encoding aromatic amino-transferases I and II reveals a new aminotransferase subfamily. Mol. Gen. Genet. 257, 238–248.
Kabsch, W., 2010. Xds. Acta Crystallogr. D-Biol. Crystallogr. 66, 125–132.
Karsten, W.E., Reyes, Z.L., Bobyk, K.D., Cook, P.F., Chooback, L., 2011. Mechanism of the aromatic aminotransferase encoded by the Aro8 gene from Saccharomyces cerevisiea. Arch. Biochem. Biophys. 516, 67–74.
Kradolfer, P., Niederberger, P., Hutter, R., 1982. Tryptophan degradation in saccharomyces-cerevisiae – characterization of 2 aromatic aminotransferases. Arch. Microbiol. 133, 242–248.
Langer, G., Cohen, S.X., Lamzin, V.S., Perrakis, A., 2008. Automated macromolecular model building for X-ray crystallography using ARP/wARP version 7. Nat. Protoc. 3, 1171–1179.
Mccoy, A.J., Grosse-Kunstleve, R.W., Adams, P.D., Winn, M.D., Storoni, L.C., Read, R.J., 2007. Phaser crystallographic software. J. Appl. Crystallogr. 40, 658–674.
Mueller, U., Forster, R., Hellmig, M., Huschmann, F.U., Kastner, A., Malecki, P., Puhringer, S., Rower, M., Sparta, K., Steffien, M., Uhlein, M., Wilk, P., Weiss, M.S., 2015. The macromolecular crystallography beamlines at BESSY II of the Helmholtz-Zentrum Berlin: Current status and perspectives. Eur. Phys. J. Plus 130.
Murshudov, G.N., Vagin, A.A., Dodson, E.J., 1997. Refinement of macromolecular structures by the maximum-likelihood method. Acta Crystallogr. D-Biol. Crystallogr. 53, 240–255.
Paiardini, A., Bossa, F., Pascarella, S., 2004. Evolutionarily conserved regions and hydrophobic contacts at the superfamily level: the case of the fold-type I, pyridoxal-5'-phosphate-dependent enzymes. Protein Sci. 13, 2992–3005.
Rzad, K., Gabriel, I., 2015. Characterization of two aminotransferases from Candida albicans. Acta Biochim. Pol. 62, 903–912.
Rzad, K., Milewski, S., Gabriel, I., 2018. Versatility of putative aromatic amino-transferases from Candida albicans. Fungal Genet. Biol. 110, 26–37.
Tomita, T., Miyagawa, T., Miyazaki, T., Fushinobu, S., Kuzuyama, T., Nishiyama, M., 2009. Mechanism for multiple-substrates recognition of alpha-aminoadipate amino-transferase from Thermus thermophilus. Proteins 75, 348–359.
Urrestarazu, A., Vissers, S., Iraqui, I., Grenson, M., 1998. Phenylalanine- and tyrosine-auxotrophic mutants of Saccharomyces cerevisiae impaired in transamination. Mol. Gen. Genet. 257, 230–237.
Winn, M.D., Ballard, C.C., Cowtan, K.D., Dodson, E.J., Emsley, P., Evans, P.R., Keegan, R.M., Krissinel, E.B., Leslie, A.G.W., McCoy, A., McNicholas, S.J., Murshudov, G.N., Pannu, N.S., Potterton, E.A., Powell, H.R., Read, R.J., Vagin, A., Wilson, K.S., 2011. Overview of the CCP4 suite and current developments. Acta Crystallogr. D-Biol. Crystallogr. 67, 235–242.